Published in IET Microwaves, Antennas & Propagation
Received on 26th January 2012
Revised on 25th July 2012
doi: 10.1049/iet-map.2012.0055

ISSN 1751-8725

Dual-band antenna with highly isolated outputs for global navigation satellite systems receivers

M.V.T. Heckler[1] *E.N. Lavado*[2] *W. Elmarissi*[3] *N. Basta*[3] *A. Dreher*[3]

[1]*Universidade Federal do Pampa (UNIPAMPA), Av. Ibirapuita, 810, 97546-550 Alegrete, RS, Brazil*
[2]*Universitat Politècnica de Catalunya (UPC), Jordi Girona 1-3, 08034 Barcelona, Spain*
[3]*German Aerospace Center (DLR), Oberpfaffenhofen, 82234 Wessling, Germany*
E-mail: marcos.heckler@unipampa.edu.br

Abstract: This study describes the design of a dual-band microstrip antenna with four isolated outputs. The proposed antenna has been optimised to operate in the E5a/E5b and E1 bands of the European satellite navigation system Galileo. Each pair of outputs delivers the signal in only one of the operating bands; hence the antenna operates also as a diplexer. The operation principle, the design procedure and measured results are presented and discussed. It is demonstrated by means of measured results that the designed antenna exhibits high isolation between its output ports and that good performance in terms of radiation pattern and polarisation purity was obtained.

1 Introduction

The number of applications that rely on satellite navigation systems has strongly increased in the last decade. Global navigation satellite systems (GNSS), such as GPS, GLONASS and the future European Galileo system, find many uses in civil and military applications. Especially for safety-of-life (SoL) applications, GNSS receivers must exhibit high robustness and deliver highly precise positioning. Such a performance depends on several parameters of the whole receiver chain. Some of the critical issues regarding the antenna for high-precision GNSS are phase behaviour, polarisation purity and multi-band operation.

For good performance, phase variations introduced by the antenna radiation pattern must be known a priori. Antenna phase characteristics can then be taken into account during the signal processing so that the proper compensations can be made. Polarisation purity not only increases the overall signal-to-noise ratio of the receiver, but also improves immunity against reception of multi-path signals, which can degrade the accuracy of the position estimation. Dual-band operation increases robustness and the precision of the positioning. For the Galileo system, two interesting bands are E5a/E5b (1164–1215 MHz) and E1 (1559–1591 MHz).

Since GNSS signals are received normally at power levels well below the noise, the receiver chain must exhibit high gain, hence filtering of out-of-band interference becomes a critical issue. There are several systems that operate near the E5 and E1 bands. Examples of such systems are civil and military high power pulsed radar systems and distance measuring equipment. Mobile phone systems are also of interest, especially those working at around 1.7 GHz. Suppressing out-of-band interference must be considered in the design of robust GNSS receivers, so as to guarantee good performance continuously. For example, in a receiver with the topology shown in Fig. 1*a*, the only filtering performed before the low-noise amplifier (LNA) relies on the frequency selectivity of the antenna. If the antenna properties are not narrow banded, the signal radiated by a mobile phone in the vicinity of the receiver or a high power pulsed radar may damage the LNA permanently and bring the GNSS receiver out of operation.

Addition to the use of an antenna with selective properties, system robustness can be further improved by separating the bands already at the beginning of the receiver chain, in order for them to be independent from each other already in the analogue domain. As suggested in Fig. 1*a*, frequency split is commonly done by using a diplexer which introduces additional insertion loss, hence increasing the overall receiver noise figure. Alternatively, an antenna that separates and delivers each band of interest to different and isolated ports is highly desirable for SoL GNSS applications. This is the case of the receiver described in the block diagram shown in Fig. 1*b* [1].

Several geometries have been proposed for the design of GNSS antennas [1–13]. In most of the dual-band designs, the antenna has only one output that delivers both operation bands. The geometry described in [5], however, divides the GPS and the satellite digital multimedia broadcasting bands into two different ports, but the level of isolation between the two outputs at the GPS band is around 5 dB only, which is not suitable for many applications. Another geometry that exhibits dual-band operation and presents two outputs has been recently published in the literature [6], where one single patch is fed with two pairs of slots. Each pair is used to feed the patch at different frequencies. Circular polarisation is obtained by means of two 90°

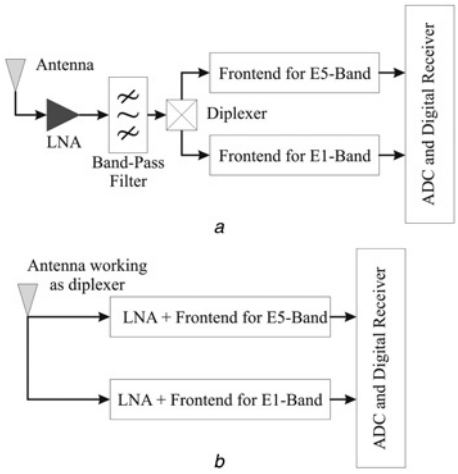

Fig. 1 *Two different approaches for dual-band reception*

a Receiver with diplexer
b Proposed approach

hybrids that have been optimised for each band and have been placed below the ground plane (GND) containing the slots. The main drawback of this geometry is that it is only feasible if the two operation bands are located far away from each other. This limitation is not suitable for GNSS, where all the operating bands currently in use are located inside the L band.

In order to obtain a geometry that satisfies the requirements for SoL systems as stated above, a novel microstrip antenna architecture for the future European Galileo system has been developed. In contrast to other dual-band circularly polarised antennas described in the literature, which couple the signals of both operating bands to only one output, the antenna described in this paper separates the E5a/E5b and the E1 bands in isolated ports. This feature has been achieved with two stacked patches and different feeding techniques for each frequency band. In [14], the authors presented simulation results of such an antenna without describing deeply the details for the antenna design. Measurements showed that additional optimisation is necessary from the geometry presented in [14]. In [1], the concept of an antenna working as a diplexer was proposed, but the design parameters of the proposed antenna were not described in detail. In the next section, the geometry of the proposed antenna is described and its operation principles and main design parameters are discussed. The redesign has been carried out by means of experimental optimisation, which is addressed in Section 5. Finally, measured results of the optimised antenna are presented, indicating that good polarisation purity and high isolation between the ports are obtained.

2 Antenna design

Owing to their low aerodynamic profile, ease of construction and low cost especially for mass production, microstrip antennas are very suitable for the proposed application. Circular polarisation operation can be obtained with microstrip antennas by means of several methods [4]. The simplest technique is by means of exciting two orthogonal modes in the same patch with only one feeding port and geometry perturbation [4]. Examples are the nearly square patch and the corner-truncated square patch. Despite their design simplicity, such geometries are normally very sensitive to construction and material tolerances. Besides, they present narrow axial ratio bandwidth and, if used to build an antenna array, mutual coupling will degrade polarisation purity substantially. Hence, such radiators are not suitable for the intended application.

The proposed antenna is composed of two stacked patches to obtain the dual-band characteristic [1, 14]. For circular polarisation operation, two orthogonal modes are excited with each patch. The 90° phase shift can be introduced by using external hybrids. The stack-up of the proposed antenna is shown in Fig. 2, where the top patch will resonate in the upper frequency band (E1) while the bottom patch operates at the lower frequencies (E5a/E5b). The dielectric materials have been chosen in order to achieve wide radiation patterns, according to the analysis performed in [15]. The patches are fed by two different feeding mechanisms, so that no coupling between them is needed to achieve dual-band properties as it is necessary in the case of conventional stacked patch arrangements. The energy of the incoming wave in the E1 band is received by the top patch, which is electrically connected to the feed lines by means of two vias, whereas the energy of the E5a/E5b wave is received through two apertures by the bottom patch. A schematic top view is shown in Fig. 3. One hole for each via has been drilled in the bottom patch so that no electric contact exists between it and the vias.

The bottom patch is fed through electromagnetic coupling due to constructive and performance reasons. Feeding the bottom patch with vias would demand the use of blind vias, which are more difficult to manufacture. Moreover, the use of vias would include a series inductance in the bottom patch input impedance, hence reducing its bandwidth.

Circular polarisation operation is obtained by exciting two orthogonal modes (TM_{01} and TM_{10}) with each patch, so that two feeding points are required for each frequency band.

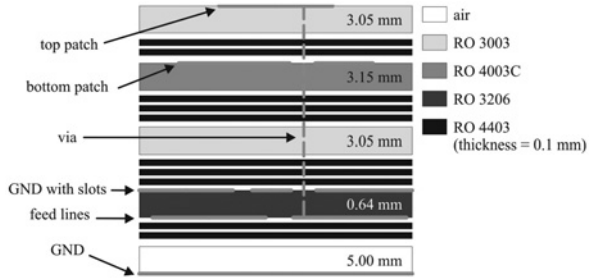

Fig. 2 *Stack-up of the described antenna*

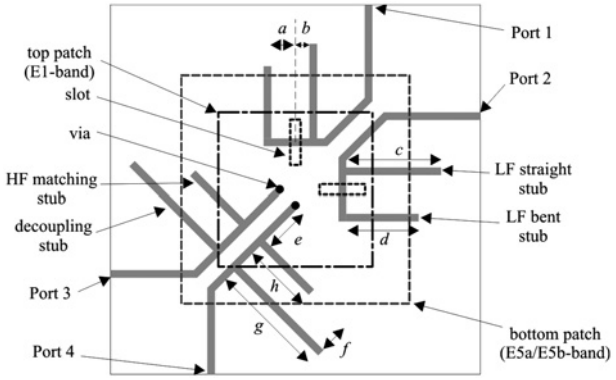

Fig. 3 *Top view of the designed antenna*

All dimensions are given in the text

doi: 10.1049/iet-map.2012.0055

Right-handed circular polarisation (RHCP) is finally obtained by introducing a 90° phase shift between the two TM modes, which can be achieved using a 90°-hybrid optimised to work at the centre of each desired band. For the proposed case, the operation of the hybrids will be satisfactory, provided that good isolation is obtained between the two ports operating in the same band.

The input impedance of the lower patch is dependent on several parameters. The location of the slots was chosen off-centre to allow placing all the feed lines in the same level of the multilayer structure. The slot positions were chosen so as to improve isolation between ports 1 and 2. The lengths of the slots play an important role on both the input impedance and power loss by excitation of surface waves. The longer the slots, the larger the input resistance and the higher is the power lost due to surface waves. Therefore the slot lengths were optimised as a compromise between input resistance, which should not be too low so as to make impedance matching realisable, and loss due to surface waves. The impedance matching is obtained by employing open-ended stubs. Two stubs have been used to match the impedance to 50 Ω at ports 1 and 2. Matching can be achieved by adjusting the lengths of the low frequency (LF) straight stub and LF bent stub without the need of changing the distance between them and their positions relative to the slots. Fig. 4 presents the variation of the input impedance at the slots level when the lengths of the LF bent stubs are varied and for $c = 0$ (see Fig. 3). One can see that the bent stub adds a series reactance in the input impedance. Fig. 5 shows the variation of the input impedance as a function of the length of the LF straight stubs. The impedance is calculated at the connection of the stub to the feed line. One can see that this stub produces a shunt susceptance, which can be adjusted to match finally the input admittances at ports 1 and 2.

The top patch is fed by means of vias, the distances of which from the patch centre govern the input impedance as in an ordinary patch antenna. However, in the present case, the vias positions have direct impact on the isolation between all the ports. The isolation between ports 3 and 4 can be improved by placing the vias close to the patch edges. On the other hand, the positions of the vias have also impact on the isolation between ports 1 and 2, which is improved by placing the vias close to the patch centre, as shown in Fig. 6. Matching at ports 3 and 4 is achieved with two stubs, which are named here as high frequency (HF) matching stub and decoupling stub (see Fig. 3). The last one is $\lambda_g/4$-long, where λ_g is the guided wavelength at 1.189 GHz, so as to act as short circuit at the central frequency of the E5a/E5b band at the point the stubs are connected to the feed lines. This causes strong reflection of the E5a/E5b band signals, hence isolating ports 3 and 4 from ports 1 and 2 in the frequency range of E5a/E5b band. The length and the position of the HF matching stub are adjusted to finally match the input impedance of the top patch.

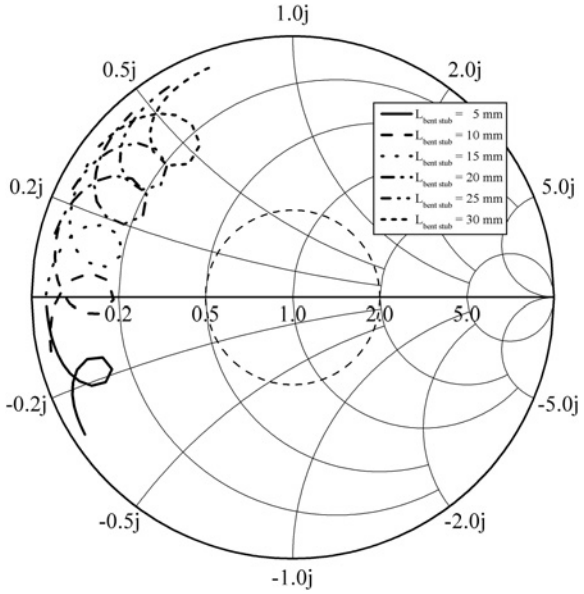

Fig. 4 *Variation of the input impedance at the slot plane for different lengths of the bent stub*

Simulations were done considering $b = 6.03$ mm, $c = 0$ mm, $e = 9.18$ mm, $f = 2.35$ mm, $g = 30$ mm and $h = 10.55$ mm (see Fig. 3)

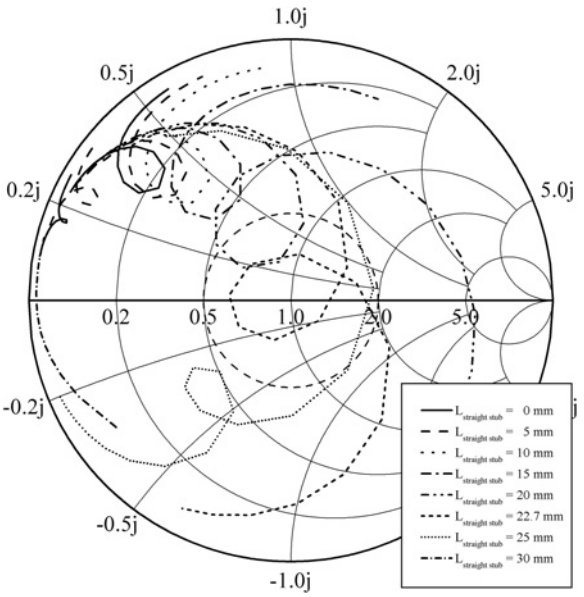

Fig. 5 *Variation of the input impedance at connection of the straight stub to the feed line for different lengths of the straight stub*

Simulations were done considering $a = 7.33$ mm, $b = 6.03$ mm, $d = 14.66$ mm, $e = 9.18$ mm, $f = 2.35$ mm, $g = 30$ mm and $h = 10.55$ mm (see Fig. 3)

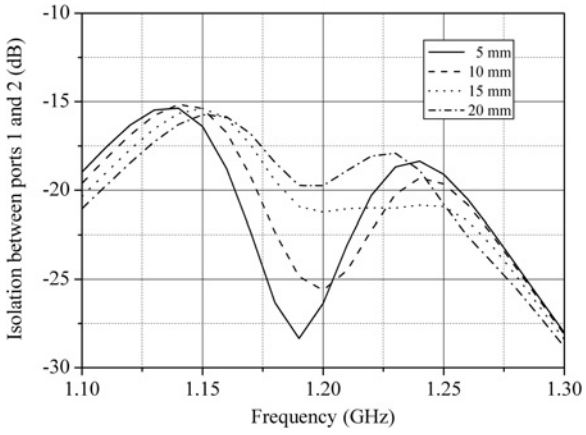

Fig. 6 *Variation of the isolation between ports 1 and 2 as a function of the vias positions from the structure geometrical centre*

Simulations were done considering $a = 7.33$ mm, $b = 6.03$ mm, $c = 22.49$ mm, $d = 14.66$ mm, $e = 9.18$ mm, $f = 2.35$ mm, $g = 30$ mm, $h = 10.55$ mm (see Fig. 3)

The antenna dimensions were optimised using the Ansoft HFSS [16]. The top and the bottom patches have square shapes and edge sizes of 52.80 and 63.10 mm, respectively. Each slot is displaced 20.00 mm from the structure centre and is 2.00 mm wide and 19.20 mm long. The vias connecting the feed lines to the top patch are positioned 10.00 mm off the structure centre. The main dimensions of the feeding system are the following (see Fig. 3): $a = 8.33$ mm, $b = 6.03$ mm, $c = 22.49$ mm $d = 14.66$ mm, $e = 9.18$ mm, $f = 2.35$ mm, $g = 30$ mm and $h = 11.7$ mm. All feed lines present a characteristic impedance of 50 Ω and are 0.95 mm wide.

3 Fabrication

A prototype of the proposed antenna has been built and is shown in Fig. 7. The comparison between the simulated and measured input impedance for ports 3 and 4 (E1 band) showed good agreement. However, a large discrepancy between computed and measured results has been observed for ports 1 and 2, as it can be seen from the reflection coefficient curves shown in Fig. 8. All the prototype dimensions have been checked with a microscope and the only discrepancies lower than 25 μm from the nominal values have been verified. This deviation has been considered acceptable for the etching process adopted to build the prototypes and is small enough to cause only little performance degradation at L band. The designed antenna has been analysed using the Ansoft Designer as well, which provided similar results than the ones obtained with HFSS. Few parametric simulations confirmed that such fabrication imperfections have only little influence on the prototype performance. X-ray imaging was used to inspect the internal parts of the prototype to assess possible misalignment between the multiple copper layers, but no apparent problem has been detected as well. In order to assess whether the cause for the discrepancy observed in Fig. 8*a* was due to material properties, a parametric study has been carried out by varying the dielectric constant of the different substrates that compose the multilayer structure of the proposed antenna.

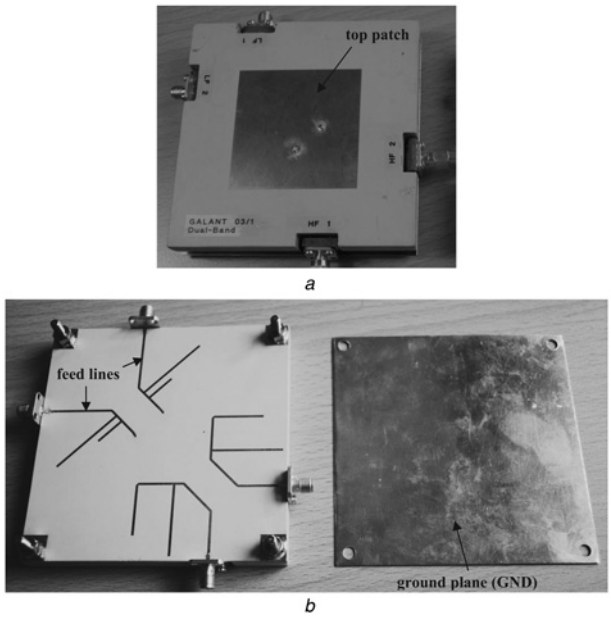

Fig. 7 *Manufactured prototype*

a Top view
b Bottom view

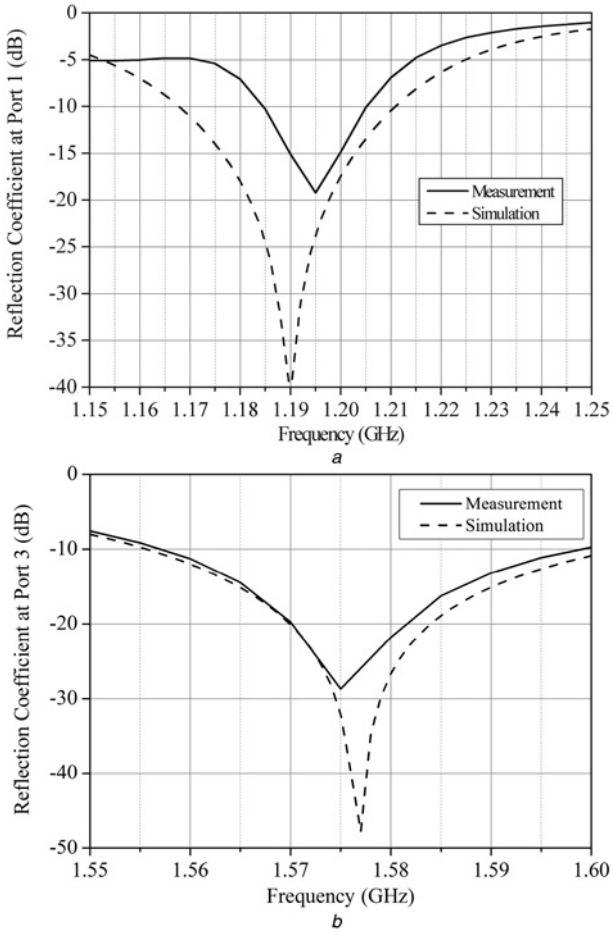

Fig. 8 *Comparison between simulated and measured reflection coefficient*

a At port 1
b At port 3

4 Parametric studies

In order to assess the performance deviations due to material tolerances, a sensitivity study was conducted regarding the dielectric constant ε_r of three laminates employed in the proposed design: RO3003 ($\varepsilon_r = 3.00 \pm 0.04$), RO3206 ($\varepsilon_r = 6.15 \pm 0.15$) and RO4003C ($\varepsilon_r = 3.55 \pm 0.05$). The tolerances of ε_r have been taken from the datasheet provided by the manufacturer. The dielectric constants of the substrate materials have been swept individually, while keeping the other two at nominal values. Simulated results are presented in Fig. 9, where one can see that the largest deviation is obtained when the dielectric constant of the laminate RO 3206 is varied. However, the performance is not changed so drastically to justify the discrepancy as shown in Fig. 8.

According to [17], the value of the dielectric constant of practical microwave laminates that should be considered during the design of a microwave device, depends on different factors, such as the substrate thickness, roughness of the copper clad and the material anisotropy. Measuring the dielectric constant may help designers to obtain better agreement between the experimental results and the numerical predictions. However, the measured value for ε_r

doi: 10.1049/iet-map.2012.0055

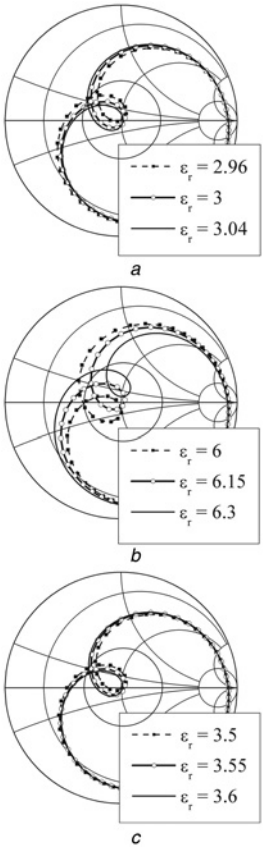

Fig. 9 *Input impedance at port 1 for different values of dielectric constants for*

a RO3003
b RO3206
c RO4003C

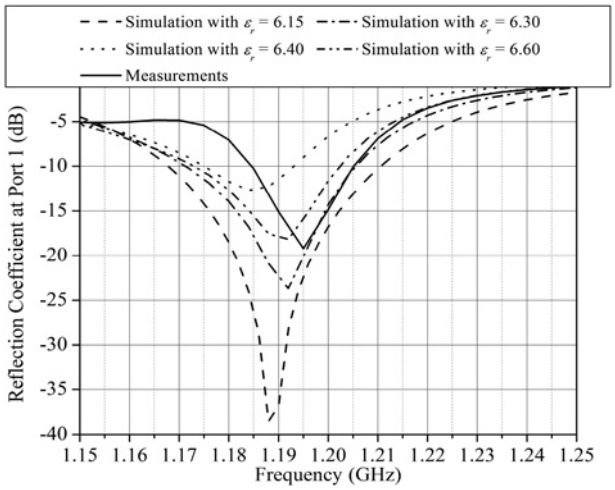

Fig. 10 *Reflection coefficient at port 1 for different values of dielectric constants for RO3206*

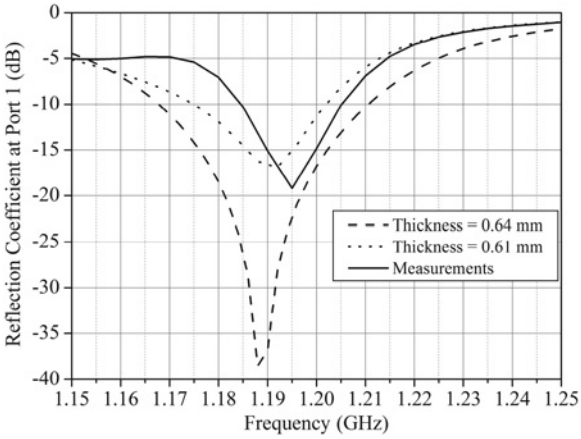

Fig. 11 *Reflection coefficient at port 1 for different thicknesses for RO3206*

depends on the test method used to characterise the laminate [17]. For this reason, the nominal value of ε_r, as given in the laminate datasheet, may not represent the dielectric constant for the case of the designed antenna. From the parametric analyses shown in Fig. 9, it was found that variations in the RO3206 layer resulted in the greatest changes in the antenna impedance matching. Therefore additional simulations were done by increasing the dielectric constant up to $\varepsilon_r = 6.60$, which is considered by the substrate manufacturer as a good value for practical designs [18]. The results are shown in Fig. 10, where one can see that the curve behaviour for $\varepsilon_r = 6.40$ fairly approximates the experimental result. Another analysis was performed by considering the nominal value of the dielectric constant of RO3206, but by varying the laminate thickness. This could be the case resulting from over pressuring during the fabrication process of the multilayer structure. The results are shown in Fig. 11, where the experimental data could not be accurately modelled by varying this parameter.

A second prototype was built to assess whether there were problems during the fabrication process. However, measured results similar to the solid curve shown in Fig. 8 have been obtained. From the results obtained, the discrepancies could be attributed only to some material property that was not fully modelled by the used software, such as some degree of anisotropy present in the laminates. Indeed, the lower patch is fed by striplines coupled to slots in the GND. Anisotropy will influence the antenna characteristics, since the electric field at the striplines in regions away from the apertures are predominantly oriented along the normal direction to the substrate plane, whereas the fields in the slots are oriented parallel to the GND. Hence, the electric fields in these two regions will be subject to different dielectric constants if anisotropy is present. A moderate degree of anisotropy may deteriorate the antenna performance in comparison to the simulated isotropic structure.

According to [17], RO3206 exhibits anisotropic behaviour with ε_r values of 8.17 and 6.27 along the x–y plane and along the z-axis, respectively. This may be one of the main factors governing the performance degradation of the prototype in comparison to the designed characteristics. As anisotropic materials cannot be modelled in the electromagnetic simulators used for the presented antenna design, an experimental optimisation has been carried out and is described next.

5 Experimental optimisation

The experimental optimisation has been done by adjusting the length of the straight and the bent stubs used in the feeding system for the bottom patch. This process has been carried out step by step in order to avoid shortening the stubs beyond the need, which could damage the prototype permanently. The access to the feed lines was possible because the lowest GND (Fig. 2) was made removable. The

Table 1 Variation of the stubs during the experimental optimisation of the antenna (Fig. 3)

Iteration	*c* (mm)	*d* (mm)	*h* (mm)
0	22.49	14.66	11.68
1	21.80	14.66	11.68
2	21.15	14.66	11.68
3	21.15	13.80	11.68
4	21.15	13.80	10.55

stubs have been gradually cut out according to the iterations listed in Table 1, where the lengths of the three stubs for impedance matching are given. A computer code has been implemented by using the transmission line theory, which was used to calculate the de-embedded impedance at the plane of the straight stub (for ports 1 and 2). This allowed estimating the new stub dimension after every iteration. The measured results for input impedance are shown in Fig. 12. One can observe that only few iterations were needed in the optimisation process due to the technique employed. Iteration 4 was necessary to produce a slight frequency shift on the input impedance at ports 3 and 4. From Fig. 12, one can see that a change in the HF feeding lines had nearly no influence in the input impedance seen at ports 1 and 2 at the E5a/E5b band, hence confirming that the E1 and E5a/E5b ports are highly isolated from each other.

After the experimental optimisation, the *S*-parameters were measured. The results are shown in Figs. 13 and 14. Owing to the symmetry of the structure, only four *S*-parameters are given. One can see that the reflection coefficients at the four ports are below −10 dB in the respective operation bands. Moreover, the isolation between ports 4 and 1, and ports 3 and 1, are larger than 23 dB in the entire L band (see dotted and dashed curves in Fig. 14).

The measured radiation patterns are shown in Figs. 15 and 16. For the measurements, two external 90°-hybrids (part number ZX10Q-2-19 manufactured by Mini-Circuits®) have been used to produce the necessary phase shift between the ports 1 and 2 and ports 3 and 4, so that the antenna

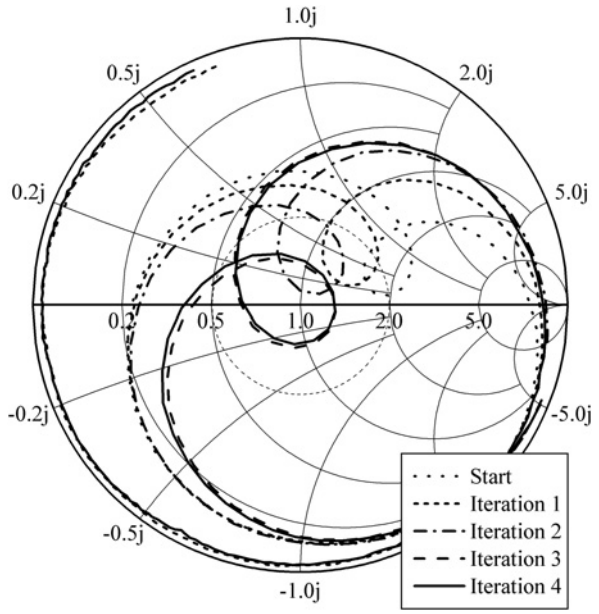

Fig. 12 *Experimental optimisation of the input impedance at the LF port*

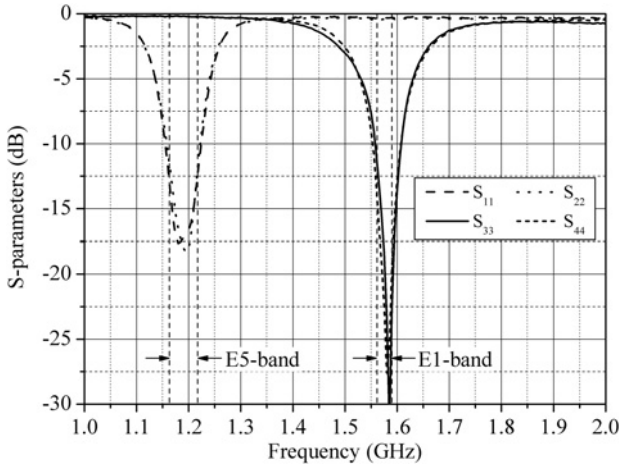

Fig. 13 *Measured reflection coefficient at the four antenna outputs*

The dashed lines indicate the two operating bands: E5a/E5b (1.164–$1.215 GHz) and E1 (1.559–1.591 GHz)

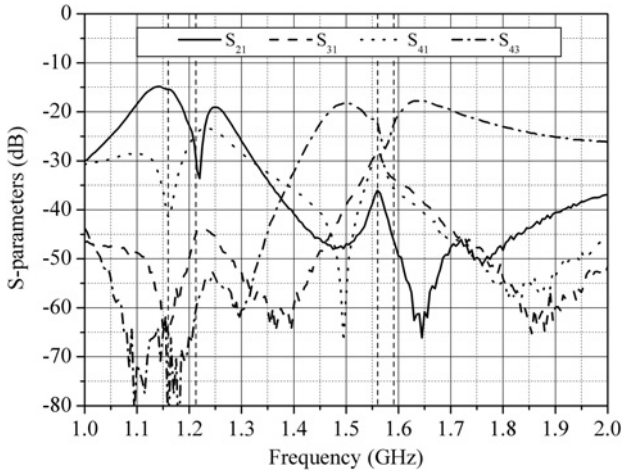

Fig. 14 *Measured isolation between some of the output ports*

Owing to the structure symmetry, only four *S*-parameters are shown. The dashed lines indicate the two operating bands: E5a/E5b (1.164–1.215 GHz) and E1 (1.559–1.591 GHz)

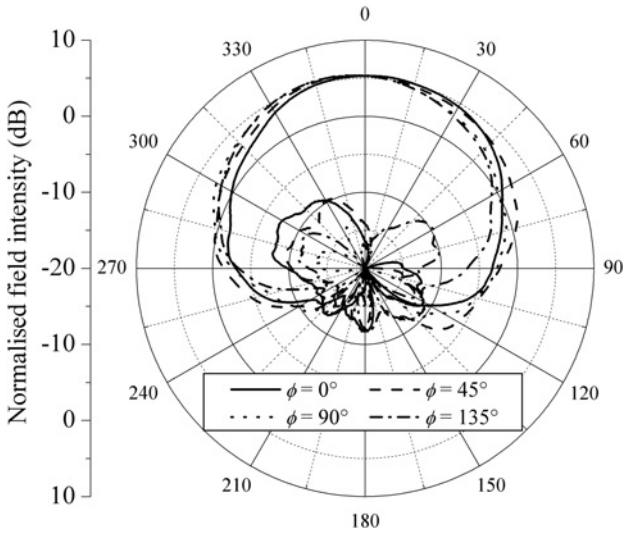

Fig. 15 *Measured gain pattern at 1189 MHz for different azimuth (ϕ) planes*

Solid lines are RHCP and dashed lines are left-handed circular polarisation (LHCP)

doi: 10.1049/iet-map.2012.0055

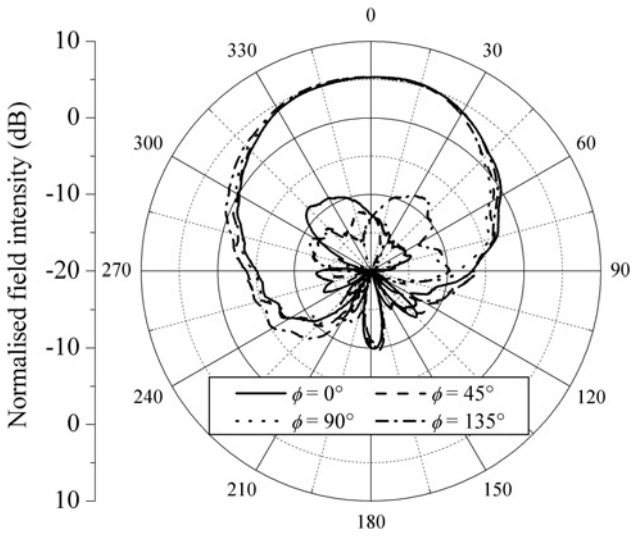

Fig. 16 *Measured gain pattern at 1575 MHz for different azimuth (ϕ) planes*

Solid lines are RHCP and dashed lines are LHCP

operates with circular polarisation. At both mid-frequencies, measured values of axial ratio equal to 1.7 dB were obtained. For comparison purposes, the simulated result was 1.0 dB for both mid-frequencies. The discrepancy between measured and simulated values can be attributed to several reasons, such as the tolerances in the fabrication process and the properties of the dielectrics. One can also observe that broad radiation patterns were obtained, which is an important requirement for GNSS. Half-power beam widths of 91° and 86°, respectively, for the E5a/E5b and the E1 bands were verified and a maximum gain drop of 12 dB from the zenith to the horizon has been obtained. The maximum gain was 5.3 dBic for the central frequencies of both bands. Another important feature of the radiation properties of the designed antenna is the symmetry of the pattern at different azimuth angles in both bands.

Finally, a frequency sweep has been performed and the gain in the broadside direction has been measured. The results are presented in Fig. 17. By examining the co-polarisation curves, one can see that isolation larger than

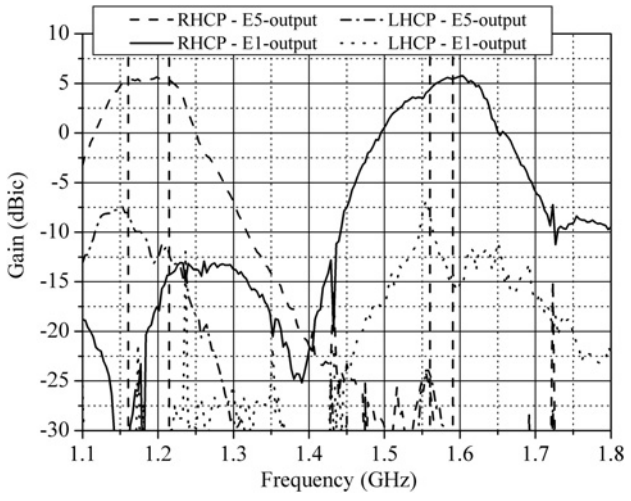

Fig. 17 *Measured gain at boresight as a function of frequency*

The dashed lines indicate the two operating bands: E5a/E5b (1.164–1.215 GHz) and E1 (1.559–1.591 GHz)

20 dB was obtained between the output ports for E5a/E5b and E1 bands. Furthermore, a gain drop larger than 10 dB has been obtained from the mid band of E1 to the GSM band above 1.7 GHz.

6 Conclusion

The design process of a novel dual-band microstrip antenna with highly isolated outputs has been discussed in this paper. Discrepancies between the numerical and experimental results were verified and they could neither be related to problems in the construction nor to the material tolerances given in the datasheet of the employed microwave laminates. Since the computer model could not reproduce the measured results, an experimental optimisation was carried out as a part of the design process. Measurements of the optimised prototype show that very good performance has been finally obtained. Moreover, high isolation between the antenna outputs has been verified. The antenna has been already used successfully for field tests with a GNSS receiver [1].

Even though computer modelling keeps advancing fast with the improvement of computational power, the results shown in this paper indicate that the experimental verification should still be part of the design process of novel antennas. Despite the application of full-wave tools during the initial stage of the proposed design, good performance could not be obtained with the antenna dimensions optimised by simulations. The experimental optimisation that has been conducted in this work was necessary to compensate for deviations in the material properties, which may not appear in the datasheets of commercial microwave laminates.

7 References

1 Heckler, M.V.T., Cuntz, M., Konovaltsev, A., Greda, L.A., Dreher, A., Meurer, M.: 'Development of robust safety-of-life navigation receivers', *IEEE Trans. Microw. Theory Tech.*, 2011, **59**, (4), pp. 998–1005
2 Pozar, D.M., Duffy, S.M.: 'A dual-band circularly polarized aperture-coupled stacked microstrip antenna for global positioning satellite', *IEEE Trans. Antennas Propag.*, 1997, **45**, (11), pp. 1618–1625
3 Boccia, L., Amendola, G., di Massa, G.: 'A dual frequency microstrip patch antenna for high-precision GPS applications', *IEEE Antennas Wirel. Propag. Lett.*, 2004, **3**, pp. 157–160
4 Garg, R., Bhartia, P., Bahl, I., Ittipiboon, A.: 'Microstrip antenna design handbook' (Artech House, 2001)
5 Oh, J.-H., Hong, Y.-P., Yook, J.-G.: 'Dual circularly-polarized stacked patch antenna for GPS/SDMB'. 2008 IEEE Int. Symp. on Antennas and Propagation, San Diego, USA, July 2008
6 Ferrero, F., Luxey, C., Jacquemod, G., Staraj, R.: 'Dual-band circularly polarized microstrip antenna for satellite applications', *IEEE Antennas Wirel. Propag. Lett.*, 2005, **4**, pp. 13–15
7 Baracco, J.-M., Salghetti-Drioli, L., de Maagt, P.: 'AMC low profile wideband reference antenna for GPS and Galileo systems', *IEEE Trans. Antennas Propag.*, 2008, **56**, (8), pp. 2540–2547
8 Wang, Z., Fang, S., Fu, S., Lü, S.: 'Dual-band probe-fed stacked patch antenna for GNSS applications', *IEEE Antennas Wirel. Propag. Lett.*, 2009, **8**, pp. 100–103
9 Boccia, L., Amendola, G., di Massa, G.: 'Performance evaluation of shorted annular patch antennas for high-precision GPS systems', *IET Microw. Antennas Propag.*, 2007, **1**, (2), pp. 465–471
10 Abbasi, N.A., Langley, R.J.: 'Multiband-integrated antenna/artificial magnetic conductor', *IET Microw. Antennas Propag.*, 2011, **5**, (6), pp. 711–717
11 Lee, C.K., Teo, P.T., Luo, X.F.: 'Frequency-selective surfaces for GPS and DCS1800 mobile communication, 2nd part: integration with antenna for scattering reduction', *IET Microw. Antennas Propag.*, 2007, **1**, (2), pp. 322–327
12 Huang, C.-Y., Ling, C.-W., Kuo, J.-S.: 'Dual-band microstrip antenna using capacitive loading', *IEE Proc. Microw. Antennas Propag.*, 2003, **150**, (6), pp. 401–404

13 Su, C.-M., Wong, K.-L.: 'A dual-band GPS microstrip antenna', *Microw. Opt. Tech. Lett.*, 2002, **33**, (4), pp. 238–240
14 Heckler, M.V.T., Lavado, E.N., Dreher, A.: 'Dual-band circularly polarized microstrip antenna with two isolated outputs suitable for navigation systems'. 2009 IEEE Int. Symp. on Antennas and Propagation, Charleston, USA, June 2009
15 Heckler, M.V.T., Elmarissi, W., Greda, L.A., Cuntz, M., Dreher, A.: 'Narrow-band microstrip antenna array for a robust receiver for navigation applications'. Third European Conf. on Antennas and Propagation (EuCAP 2009), Berlin, Germany, March 2009, pp. 1206–1210
16 Ansoft Corp., Ansoft HFSS version 11 – User's guide, 2008
17 Rogers Corp., General information of dielectric constants for circuit design using Rogers high frequency materials, Technical Note, 2011
18 Coonrod, J.: 'Selecting PCB materials for high frequency applications', *Microw. Eng. Eur.*, 2012, (2), pp. 18–21

doi: 10.1049/iet-map.2012.0055